Available online at www.sciencedirect.com
ScienceDirect
Journal of Power Sources 174 (2007) 1229–1233
JOURNAL OF POWER SOURCES
www.elsevier.com/locate/jpowsour

Short communication

Preparation and examination of carbon- and binder-free electrodes used in lithium-ion cells

Sun-Ho Kang, Daniel P. Abraham *

Argonne National Laboratory, Argonne, IL 60439-4837, United States

Available online 29 June 2007

Abstract

Carbon- and binder-free layered-oxide and spinel-oxide electrodes of various compositions have been prepared to determine performance degradation mechanisms of Li-ion cells that are associated with the active materials. In this work, we report the preparation of these sub-micrometer thick electrodes by a non-aqueous sol–gel spin coating on a Pt foil substrate. The active materials were characterized by various techniques including X-ray diffraction and scanning electron microscopy. Electrode properties were evaluated before and after accelerated aging by cyclic voltammetry, galvanostatic cycling and electrochemical impedance spectroscopy.
Published by Elsevier B.V.

Keywords: $LiNi_{1/3}Co_{1/3}Mn_{1/3}O_2$; $Li_{4/3}Ti_{5/3}O_4$; $LiMn_2O_4$; Characterization; Aging

1. Introduction

High-power lithium-ion batteries for hybrid electric vehicles (HEV) applications are being studied at Argonne National Laboratory (ANL) as part of the US DOE's FreedomCar and Vehicle Technologies program. Extensive tests on 18650-, prismatic-, and coin-type high-power lithium-ion cells are being conducted to identify factors that undermine their power performance and thermal safety characteristics. The investigated cells have contained a range of chemistries including layered oxides and Mn-spinels as positive electrode active materials, graphite, hard carbons and Ti-spinels as negative electrode active materials, and $LiPF_6$ and LiBOB as electrolyte salts [1–6]. The investigations are mainly conducted on composite, porous electrodes that include the active material, electronic conductive additives, and polyvinylidene difluoride (PVDF) binder.

A suite of diagnostic tools has been employed to determine the cause of cell performance degradation. These tools include the use of a Li–Sn reference wire to isolate the impedance contribution of individual electrodes [4], surface analysis techniques such as X-ray photoelectron spectroscopy to correlate changes at the electrode surfaces to electrode performance [2], and analytical electron microscopy to examine changes in the electrode bulk [1]. These data have indicated that the positive electrode is not only a dominant contributor to the impedance rise but also responsible for a portion of the capacity fade. However, identifying specific mechanisms responsible for the loss of electrode performance has been difficult; interpreting the role of the oxide materials in electrode performance degradation is also complicated by the presence of the electronic conducting carbon additives and the organic binder.

In this paper, we report the preparation, characterization, and evaluation of carbon- and binder-free (BCF) electrodes containing $LiNi_{1/3}Co_{1/3}Mn_{1/3}O_2$, $Li_{4/3}Ti_{5/3}O_4$ and $LiMn_2O_4$ active materials. Preparation of BCF film electrodes has been reported by several research groups using radio frequency (rf) magnetron sputtering [7–11], pulsed laser deposition (PLD) [12–14], electrostatic spray deposition (ESD) [15–17], and sol–gel spin coating [18–22]. Of these various experimental techniques, the sol–gel spin coating offers advantages over others in cost, ease of film preparation, and control of stoichiometry and crystallinity [18,21,22]. In this work, sub-micrometer thick BCF electrodes were prepared by non-aqueous sol–gel spin coating on a Pt foil substrate followed by heat-treatment in air. The active materials were characterized by various techniques including X-ray diffraction (XRD) and scanning electron microscopy (SEM). Electrochemical properties of the materials were evaluated by cyclic voltammetry, galvanostatic cycling and electrochemical impedance spectroscopy. Data from

* Corresponding author. Tel.: +1 630 252 4332; fax: +1 630 972 4406.
E-mail address: abraham@cmt.anl.gov (D.P. Abraham).

0378-7753/$ – see front matter. Published by Elsevier B.V.
doi:10.1016/j.jpowsour.2007.06.172

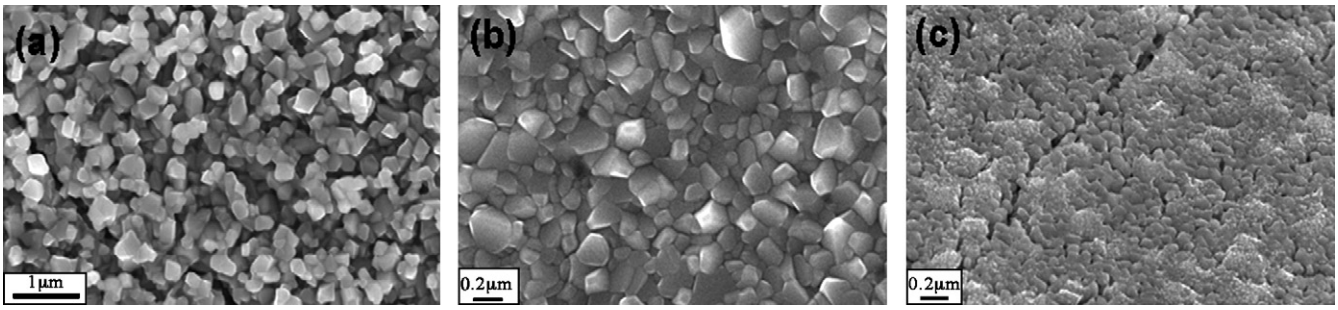

Fig. 1. SEM images of (a) $LiNi_{1/3}Co_{1/3}Mn_{1/3}O_2$, (b) $LiMn_2O_4$, and (c) $Li_{4/3}Ti_{5/3}O_4$ film electrodes.

accelerated aging experiments on the electrodes are also presented; diagnostic analysis and kinetic property measurement data on fresh and aged electrodes will be reported in future articles.

2. Electrode preparation

The $LiNi_{1/3}Co_{1/3}Mn_{1/3}O_2$ precursor sol was prepared by dissolving Li-acetate, Ni-acetate, Co-nitrate, and Mn-acetate in a mixture solution of ethanol and acetic acid. Polyvinylpyrrolidone (PVP, MW 55,000) was used as a chelating agent; PVP has been reported to be an excellent sol additive for the preparation of crack-free oxide films [19,21]. The $LiMn_2O_4$ precursor sol was prepared by dissolving Li-acetate, Mn-chloride and PVP-55000 in ethanol. The $Li_{4/3}Ti_{5/3}O_4$ precursor sol was prepared by dissolving Li-acetate, Ti-isopropoxide and PVP-55000 in an ethanol and acetic acid solution mixture. The prepared sols were spin-coated on Pt foil at 3000 rpm for 30 s to obtain a gel film. Thus prepared gel films were heat-treated at 600 °C for ~1 h in air to burn off the organic components. The spin coating and heat-treatment process were repeated several times until a film of desired thickness was obtained. Each electrode was subjected to a final heat-treatment in air to obtain the well-crystallized oxide product: the $LiNi_{1/3}Co_{1/3}Mn_{1/3}O_2$ electrode was heated at 850 °C for 2 h, the $LiMn_2O_4$ electrode at 750 °C for 3 h, and the $Li_{4/3}Ti_{5/3}O_4$ electrode at 700 °C for 30 min. After this final heat treatment, the electrodes were stored in an inert atmosphere glove box to minimize sample contamination and to prevent changes (if any) from ambient air reactions.

3. Materials characterization

Scanning electron microscopy (SEM) of the electrodes was conducted on a high-resolution Hitachi S-4700 microscope with a field emission electron source. X-ray diffraction (XRD) data were collected on a Philips powder diffractometer using Cu Kα radiation for two-theta values from 10° to 80°.

Fig. 1a–c shows morphologies of the $LiNi_{1/3}Co_{1/3}Mn_{1/3}O_2$, $LiMn_2O_4$, and $Li_{4/3}Ti_{5/3}O_4$ film electrodes, respectively. The sizes of the primary oxide particles, determined from the SEM pictures, are ~0.1–0.3 μm for $LiNi_{1/3}Co_{1/3}Mn_{1/3}O_2$ and $LiMn_2O_4$, and ~50–100 nm for $Li_{4/3}Ti_{5/3}O_4$. Note that $Li_{4/3}Ti_{5/3}O_4$ exhibits much finer primary particles; accordingly, the electrochemical active surface area of $Li_{4/3}Ti_{5/3}O_4$ is significantly greater than for the other two electrodes.

Fig. 2a–c shows the XRD patterns obtained from the $LiNi_{1/3}Co_{1/3}Mn_{1/3}O_2$, $LiMn_2O_4$, and $Li_{4/3}Ti_{5/3}O_4$ film electrodes, respectively. The most intense peaks in the diffraction patterns are from the Pt substrate. The $LiNi_{1/3}Co_{1/3}Mn_{1/3}O_2$ film (Fig. 2a) exhibits the α-$NaFeO_2$ structure (space group *R*-3*m*), which is the prototypical crystalline structure for layered $LiMO_2$ (M = transition metal atom), with small impurity peaks (denoted by *) corresponding to a cubic spinel structure such as M_3O_4 (M = Co or Mn). The integrated intensity ratio (*R*) of the (0 0 3) and (1 0 4) peaks of the $LiNi_{1/3}Co_{1/3}Mn_{1/3}O_2$ material is 1.4, which indicates that a well-layered compound with minimal cation mixing was prepared. The diffraction pattern of the $LiMn_2O_4$ film (Fig. 2b) shows the cubic spinel structure with a space group of *Fd*-3*m*. The $Li_{4/3}Ti_{5/3}O_4$ oxide film (Fig. 2c) also exhibits the diffraction pattern of cubic spinel structure (space

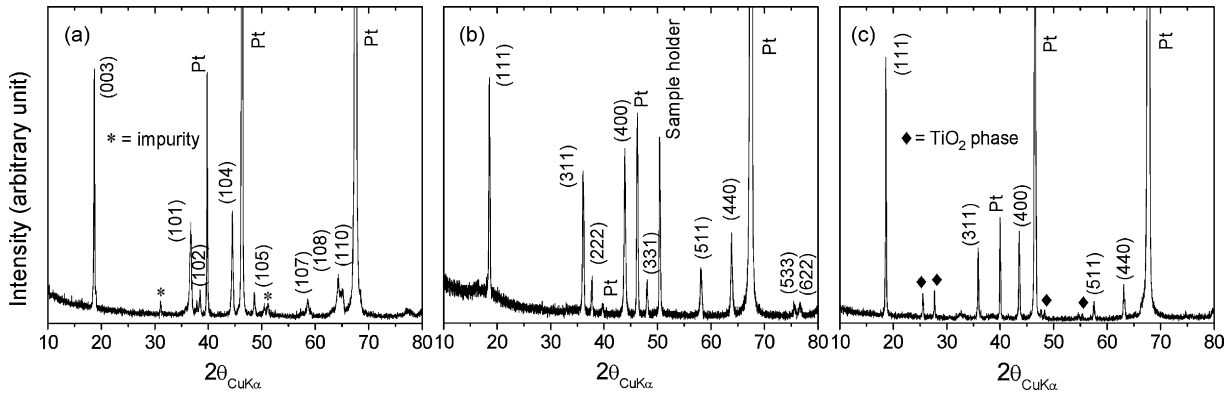

Fig. 2. XRD patterns of (a) $LiNi_{1/3}Co_{1/3}Mn_{1/3}O_2$, (b) $LiMn_2O_4$, and (c) $Li_{4/3}Ti_{5/3}O_4$ film electrodes.

group *Fd*-3*m*), with small impurity phase peaks of TiO_2 (denoted by ♦). The lattice parameters calculated from the XRD patterns of the three film electrode materials using the least square method are: $a = 0.2863 \pm 0.0004$ nm and $c = 1.424 \pm 0.002$ nm ($LiNi_{1/3}Co_{1/3}Mn_{1/3}O_2$), $a = 0.8227 \pm 0.0001$ nm ($LiMn_2O_4$), and $a = 0.8349 \pm 0.0001$ nm ($Li_{4/3}Ti_{5/3}O_4$), which are in good agreement with reported values [23–25].

4. Electrochemical evaluation

The electrochemical measurements were conducted on 2032-type coin cells (20 mm dia, 3.2 mm thick) that were assembled in an Ar-filled glove box. In addition to the oxide electrode, the cells contained a lithium metal negative electrode and Celgard 2325 separator: the electrolyte was 1 M $LiPF_6$ in a 1:1 (w/w) mixture of ethylene carbonate (EC) and diethyl carbonate (DEC). The cyclic voltammetry (CV) data were obtained at a sweep rate of 50 $\mu V\ s^{-1}$ on a Solartron 1480 MultiStat. The electrochemical impedance spectroscopy (EIS) measurements were conducted with an EG&G 273A potentiostat and a Solartron SI 1260 frequency response analyzer controlled by ZPLOT measurement software: the data were collected in the potentiostatic mode with a 10 mV perturbation about the open circuit voltage. The galvanostatic cycling data were obtained on a Maccor cycler; the coin cells were cycled at various currents in voltage ranges appropriate for each material.

4.1. Initial characterization

Fig. 3a shows a CV curve obtained from a Li/$LiNi_{1/3}Co_{1/3}Mn_{1/3}O_2$ cell in the voltage range of 2.5–4.3 V. The $LiNi_{1/3}Co_{1/3}Mn_{1/3}O_2$ material shows a simple CV curve with oxidation and reduction peaks centered at 3.8 and 3.75 V, respectively, in contrast to $LiNiO_2$-based cathode materials that show multiple peaks in the CV due to distinct phase transitions [26]. In Fig. 3b is given a CV curve of a Li/$LiMn_2O_4$ cell between 3.4 and 4.4 V. As is well known for the stoichiometric $LiMn_2O_4$ spinel material [24,27], the CV curve of the $LiMn_2O_4$ film electrode shows two distinct peaks during Li extraction/insertion from/into tetrahedral site, which is attributed to ordering of the lithium ions [24] or to cubic-to-cubic phase transition in the 4 V region [27]. Fig. 3c shows a CV curve obtained from a Li/$Li_{4/3}Ti_{5/3}O_4$ cell in the voltage range of 1.2–1.8 V. The $Li_{4/3}Ti_{5/3}O_4$ material exhibits single reduction/oxidation peak centered at ~1.55 V resulting from the lithium insertion/extraction reaction of $Li_{4/3}Ti_{5/3}O_4 + Li^+ + e^- \leftrightarrow Li_{7/3}Ti_{5/3}O_4$ [25]. The cyclic voltammograms (Fig. 3a–c), together with the XRD patterns (Fig. 2a–c), show that the targeted BCF film electrodes with layered and spinel structures were successfully fabricated by the sol–gel spin coating technique.

4.2. Aging behavior

Fig. 4 shows the charge–discharge cycling behavior of the $LiNi_{1/3}Co_{1/3}Mn_{1/3}O_2$, $LiMn_2O_4$, and $Li_{4/3}Ti_{5/3}O_4$ electrodes at 0 d and after storage at 55 °C for 36 d. The $LiNi_{1/3}Co_{1/3}Mn_{1/3}O_2$ electrode capacity decreased from an initial value of 34–23.5 μAh after the 55 °C storage at 4 V versus Li^+/Li, i.e., a ~31% capacity fade in 36 d. The $LiMn_2O_4$ electrode capacity decreased from an initial value of 151–102 μAh after the 55 °C storage at 4.12 V versus Li^+/Li, i.e., a ~32% capacity fade in 36 d. On the other hand, the $Li_{4/3}Ti_{5/3}O_4$ electrode capacity remains unchanged after the 55 °C storage at 1.55 V versus Li^+/Li.

Fig. 5 shows room-temperature EIS data obtained on the $LiNi_{1/3}Co_{1/3}Mn_{1/3}O_2$, $LiMn_2O_4$, and $Li_{4/3}Ti_{5/3}O_4$ cells before and after the 55 °C storage. The cells containing the $LiNi_{1/3}Co_{1/3}Mn_{1/3}O_2$ and $LiMn_2O_4$ electrodes show a significant impedance rise, whereas the cell containing the $Li_{4/3}Ti_{5/3}O_4$ electrode shows a decrease in impedance. Note that the EIS curve for each cell is a superposition of impedances from both the oxide and lithium metal electrodes. The observed impedance increases for the $LiNi_{1/3}Co_{1/3}Mn_{1/3}O_2$ and $LiMn_2O_4$ cells could, therefore, contain contributions from the lithium counter electrode. However, the absence of an impedance increase in the $Li_{4/3}Ti_{5/3}O_4$ electrode cell suggests that the Li counter electrode contributions to impedance increase on aging is probably small. The observed decrease in impedance on aging for the $Li_{4/3}Ti_{5/3}O_4$ cell apparently results from improved electrolyte wetting of the nano-particles (Fig. 1c) during the 55 °C storage.

The capacity decrease on cell aging reflects a depletion of cyclable lithium in the cell, which can result from several factors that include the loss of electrode active material

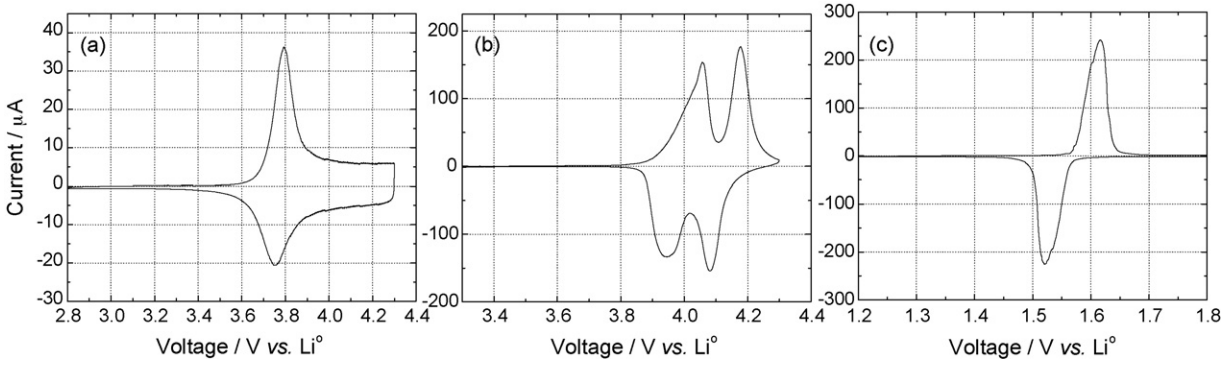

Fig. 3. Cyclic voltammograms obtained from Li cells employing the $LiNi_{1/3}Co_{1/3}Mn_{1/3}O_2$ (a), $LiMn_2O_4$ (b), and $Li_{4/3}Ti_{5/3}O_4$ (c) film materials as positive electrodes at a scan rate of 50 $\mu V\ s^{-1}$.

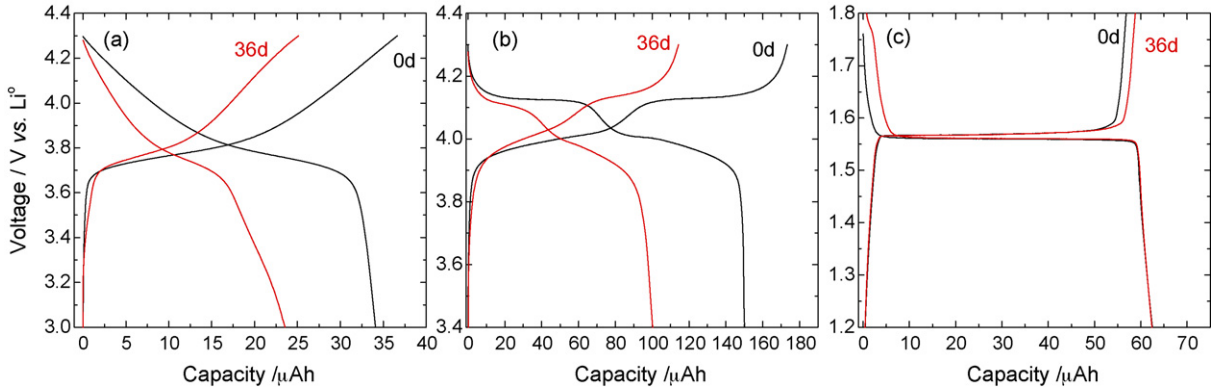

Fig. 4. Charge–discharge cycling curves (measured at RT) of (a) Li/$LiNi_{1/3}Co_{1/3}Mn_{1/3}O_2$, (b) Li/$LiMn_2O_4$, and (c) Li/$Li_{4/3}Ti_{5/3}O_4$ cells at 2 μA current (1.58 μA/cm^2) after storage at 55 °C for 0 and 36 d.

through dissolution into the electrolyte, reduction in the specific capacity because of phase changes in the material, and lithium-consuming side reactions. The capacity fade and impedance rise of the $LiMn_2O_4$ cells is most likely associated with structural degradation of the oxide: loss of Mn from the active material during cycling and aging is a well-known phenomenon [28]. The $LiNi_{1/3}Co_{1/3}Mn_{1/3}O_2$ cells capacity fade and impedance rise probably results from (a) electronic isolation of the oxide particles and (b) formation of electrode surface films that act as kinetic barriers to lithium transport at the oxide/electrolyte interface. There may also be some dissolution of the $LiNi_{1/3}Co_{1/3}Mn_{1/3}O_2$ material into the electrolyte during the 55 °C storage [28]. The unchanged capacity of the $Li_{4/3}Ti_{5/3}O_4$ cells is a testament to the remarkable integrity of the oxide under the test conditions.

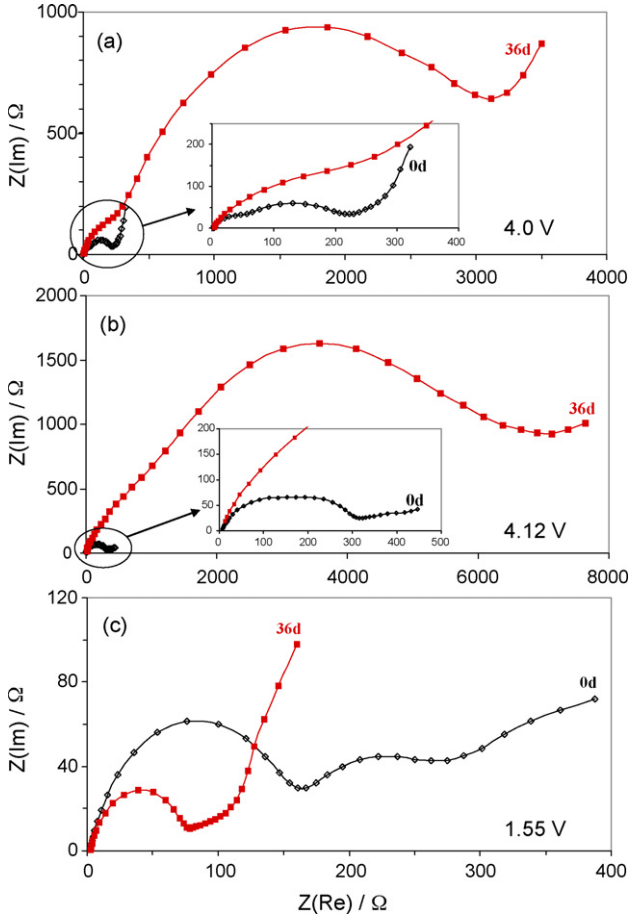

Fig. 5. EIS data (10 kHz to 10 mHz) (measured at RT) of (a) Li/$LiNi_{1/3}Co_{1/3}Mn_{1/3}O_2$ (4.0 V), (b) Li/$LiMn_2O_4$ (4.12 V) and (c) Li/$Li_{4/3}Ti_{5/3}O_4$ (1.55 V) cells after storage at 55 °C for 0 and 36 d.

Furthermore, the data reflect the absence of lithium-consuming side reactions on the 1.55 V $Li_{4/3}Ti_{5/3}O_4$ electrode: electrolyte reduction reactions responsible for the formation and growth of the solid-electrolyte interface layer on graphite particles typically occur at ≤0.8 V versus Li^+/Li. Further studies are underway to explore the origin of the observed capacity loss and impedance rise using various diagnostic techniques; these will be discussed in future publications.

5. Conclusions

Carbon and binder-free $LiNi_{1/3}Co_{1/3}Mn_{1/3}O_2$, $LiMn_2O_4$, and $Li_{4/3}Ti_{5/3}O_4$ sub-micrometer thick electrodes were prepared by a non-aqueous sol–gel spin coating on a Pt foil substrate. XRD patterns and electrochemistry data indicated that the materials had the expected crystal structures and charge–discharge cycling properties. Accelerated aging data showed capacity fade and impedance rise for the $LiNi_{1/3}Co_{1/3}Mn_{1/3}O_2$ and $LiMn_2O_4$ cells, which may result from dissolution, electronic isolation, and surface film formation on the oxide particles. The unchanged capacity of the $Li_{4/3}Ti_{5/3}O_4$ cell is in accord with the known stability of the oxide and the absence of lithium-consuming side reactions on the active material particles.

Acknowledgments

The authors thank Dennis Dees, Andrew Jansen and Gary Henrisken at Argonne National Laboratory, and Scott Maclaren, Rick Haasch and Ernest Sammann at the University of Illinois at Urbana-Champaign for their assistance and helpful discussions. This work was supported by the FreedomCAR and Vehicle Technologies Program at the U.S. Department of Energy.

The submitted manuscript has been created by the University of Chicago as Operator of Argonne National Laboratory

("Argonne") under Contract No. W-31-109-ENG-38 with the U.S. Department of Energy. The U.S. Government retains for itself, and others acting on its behalf, a paid-up, nonexclusive, irrevocable worldwide license in said article to reproduce, prepare derivative works, distribute copies to the public, and perform publicly and display publicly, by or on behalf of the Government.

References

[1] D.P. Abraham, R.D. Twesten, M. Balasubramanian, A.J. Kropf, D. Fischer, J. McBreen, I. Petrov, K. Amine, J. Electrochem. Soc. 150 (2003) A1450.
[2] M. Herstedt, D.P. Abraham, J.B. Kerr, K. Edstrom, Electrochim. Acta 49 (2004) 5097.
[3] D.P. Abraham, E.M. Reynolds, E. Sammann, A.N. Jansen, D.W. Dees, Electrochim. Acta 51 (2005) 502.
[4] D.P. Abraham, E.M. Reynolds, P.L. Schultz, A.N. Jansen, D.W. Dees, J. Electrochem. Soc. 153 (2006) 1610A.
[5] K. Amine, J. Liu, I. Belharouak, S.-H. Kang, I. Bloom, D. Vissers, G.L. Henriksen, J. Power Sources 146 (2005) 111.
[6] Z. Chen, W. Lu, J. Liu, K. Amine, Electrochim. Acta 51 (2006) 3322.
[7] N.J. Dudney, J.B. Bates, R.A. Zurh, S. Young, J.D. Robertson, H.P. Jun, S.A. Hackney, J. Electrochem. Soc. 146 (1999) 2455.
[8] Y.-I. Jang, B.J. Neudecker, N.J. Dudney, Electrochem. Solid-State Lett. 4 (2001) A74.
[9] Y.J. Park, K.S. Ryu, K.M. Kim, N.G. Park, M.G. Kang, S.H. Chang, Solid State Ionics 154 (2002) 229.
[10] H.K. Kim, T.Y. Seong, Y.S. Yoon, Electrochem. Solid-State Lett. 5 (2002) A252.
[11] C.L. Li, B. Zhang, Z.W. Fu, J. Electrochem. Soc. 153 (2006) E160.
[12] J.D. Perkins, C.S. Bahn, J.M. McGraw, P.A. Parilla, D.S. Ginley, J. Electrochem. Soc. 148 (2001) A1302.
[13] N. Kuwata, J. Kawamura, K. Toribami, T. Hattori, N. Sata, Electrochem. Commun. 6 (2004) 417.
[14] Y. Iriyama, T. Koko, C. Yada, T. Aber, Z. Ogumi, Solid State Ionics 176 (2005) 2371.
[15] C.H. Chen, E.M. Kelder, J. Schoonman, Thin Solid Films 342 (1999) 35.
[16] M. Mohamedi, A. Makino, K. Dokko, T. Itoh, I. Uchida, Electrochim. Acta 48 (2002) 79.
[17] J.L. Shui, Y. Yu, X.F. Yang, C.H. Chen, Electrochem. Commun. 8 (2006) 1087.
[18] Y.J. Park, J.G. Kim, M.K. Kim, H.T. Chung, H.G. Kim, Solid State Ionics 130 (2000) 203.
[19] Y.H. Rho, K. Kanamura, M. Fujisaki, J. Hamagami, S. Suda, T. Umegaki, Solid State Ionics 151 (2002) 151.
[20] K. Kushida, K. Kuriyama, T. Nozaki, Appl. Phys. Lett. 81 (2002) 5066.
[21] Y.H. Rho, K. Kanamura, T. Umegaki, J. Electrochem. Soc. 150 (2003) A107.
[22] J.P. Maranchi, A.F. Hepp, P.N. Kumta, Mater. Sci. Eng. B 116 (2005) 327.
[23] T. Ohzuku, Y. Makimura, Chem. Lett. 7 (2001) 642.
[24] M.M. Thackeray, Prog. Solid State Chem. 25 (1997) 1.
[25] K. Ariyoshi, R. Yamato, T. Ohzuku, Electrochim. Acta 51 (2005) 1125.
[26] J. Kim, K. Amine, Electrochem. Commun. 3 (2001) 52.
[27] Y. Shin, A. Manthiram, Chem. Mater. 15 (2003) 2954.
[28] W. Choi, A. Manthiram, J. Electrochem. Soc. 153 (2006) A1760.